HYDROACOUSTIC PROPAGATION LOSS FROM REFLECTION AND TRANSMISSION OVER SHALLOW BATHYMETRY IN THE INDIAN OCEAN

Jeffrey A. Hanson, Colin L. Reasoner, and J. Roger Bowman

Science Applications International Corporation

Sponsored by Army Space and Missile Defense Command

Contract No. W9113M-05-C-0138

ABSTRACT

We examine direct and reflected hydroacoustic waves from natural sources throughout the Indian Ocean recorded at the IMS hydroacoustic stations to help plan an experiment in the Indian Ocean using explosions deployed offshore of Western Australia. Signals have been analyzed from events with paths that cross prominent bathymetric features similar to expected experiment-to-receiver paths. Theoretical models are used to gain insight into expected experimental received levels. In addition, reflection analysis has been conducted to better understand the variables affecting signal levels from various types of reflector surfaces.

To study direct propagation over basinwide distances, waveforms from natural sources (earthquakes) are analyzed in lieu of man-made explosions. Because of the limited distribution of earthquakes along active plate boundaries within the Indian Ocean, events are used with paths that are sometimes orthogonal to the expected experiment-receiver path, but cross the same shallow bathymetric features. These include the Osborn Plateau (along the Ninety-East Ridge), Broken Ridge, and Cuvier Plateau off Western Australia. Measurements comparing hydrophone received levels at independent hydrophone stations are used to assess frequency-dependent transmission loss. The frequency-dependent attenuation is observed and quantified for hydroacoustic waves traversing the bathymetric features. Attenuation of low frequencies (2 to 15 Hz) increases as source-receiver paths shoal. A parabolic equation code is used to estimate propagation loss along the event-station path using range-dependent environmental variables. The low-frequency attenuation estimated from the models is less than observed, perhaps indicating the need to use a more complicated ocean sediment model including an elastic seafloor. The higher frequency attenuation models indicate that the starting modal structure of the signal is an important factor in the attenuation of these signals.

One key objective of the active source experiment is to improve our understanding of the factors influencing reflections of high-frequency energy. To bound the various factors, we have begun by analyzing signals from events along the Carlsberg Ridge. These shallow ridge events provide many advantages over other earthquake source regions within the Indian Ocean. The direct hydroacoustic signal is less complicated than for trench events because of the more limited area of coupling of seismic energy to hydroacoustic energy. The coupling is stronger because the sound channel axis nearly coincides with the mid-ocean ridge in this area, and the signals generally contain higher frequencies than observed elsewhere. The steep continental shelf and the seamounts that surround this area provide ample reflector surfaces to study. Reflected signals are identified and associated to reflector surfaces based on azimuth and time of arrival measurements. The power spectra of observed reflections vary between 12 and 30 dB below the direct arrival power spectrum, and reflections vary in their relative frequency content. We predict reflection strengths based on bathymetry and the source/reflector/receiver geometry. Estimates are made for both specular and diffuse type reflections. Specular reflection estimates predict much of the relative variation in peak signal strength, but the geometric model does not account for all observed variations. This discrepancy and the differences in relative frequency content indicate variations in the roughness or material properties at the reflectors.

OBJECTIVES

This project is designed to improve discrimination of underwater seismic events and improve location of hydroacoustic sources in or just above the water column. Improvement in discrimination will be achieved by empirically quantifying and theoretically modeling high-frequency (>30–50 Hz) loss of hydroacoustic energy propagating in the Sound Fixing and Ranging (SOFAR) channel from reflections off coastlines and interaction with bathymetric obstacles along path. We will also use variations in the observed residual amplitudes to identify important environmental factors that most impact high-frequency transmission loss. We will localize coastal reflector locations that will allow for better prediction of the reflected wave field. We will examine the robustness and accuracy of measuring bubble pulses from reflected or highly attenuated signals.

RESEARCH ACCOMPLISHED

A series of investigations was conducted using natural sources to address the project objectives by beginning to quantify and model loss of hydroacoustic energy propagating in the SOFAR channel from reflections off coastlines and interaction with bathymetric obstacles along path. These investigations also support detailed design of the Indian Ocean experiment, which is planned for late 2006 or early 2007.

Data are taken from recordings made by the three hydrophone stations of the International Monitoring System (IMS) that monitor the Indian Ocean basin. These stations are Cape Leeuwin, Australia, Crozet Island, and Diego Garcia (Figure 1). The Cape Leeuwin station (H01W) consists of a single triad of hydrophones, while the Crozet (H04N and H04S) and Diego Garcia (H08N and H08S) stations have two hydrophone triads each to minimize signal blockage by near-station bathymetry. Four months of continuous data for all three stations, from December 2004 to March 2005, have been made available at the U.S. Army Space and Missile Defense Command (SMDC) Monitoring Research Program (MRP) website. The majority of earthquakes used in this study are gathered from that time period, but recordings for earlier time periods when only the Cape Leeuwin and Diego Garcia stations were operational are also used. Earthquake selection is complicated by the great Sumatra earthquakes of December 26, 2004, and March 28, 2005. We attempt to limit overlapping signals by excluding earthquakes occurring in the five days after the December 2004 event, and we also select events with T-phases that have a signal-to-noise ratio (SNR) of 25 dB or greater at least one hydrophone.

Direct Transmission Paths

In order to plan the Indian Ocean experiment we would like to predict signal losses from major bathymetric features that the hydroacoustic signals will cross. A two-prong approach is taken. Observations from natural sources are analyzed, and model predictions are estimated for similar paths. Because there are few earthquakes in the experimental region, we use earthquake/station paths that cross the same features albeit at different angles. For example, a feature along the Ninety-East Ridge that we expect the experimental generated signals to cross before reaching Diego Garcia is examined using earthquakes off Sumatra recorded at Crozet. The earthquakes examined are located along the Java/Sumatra trench. There are three major clusters of events (Figure 1). The central group of events simulates paths from the experiment location to Cape Leeuwin, the northern group of events simulates the experiment location to Diego Garcia by crossing the Osborn Plateau and being recorded at Crozet, and the eastern group of events simulates the experiment location to Crozet paths that cross the Broken Ridge. The source areas have relatively unblocked paths to the southern Diego Garcia triad, H08S, and this triad is used to provide a reference signal strength.

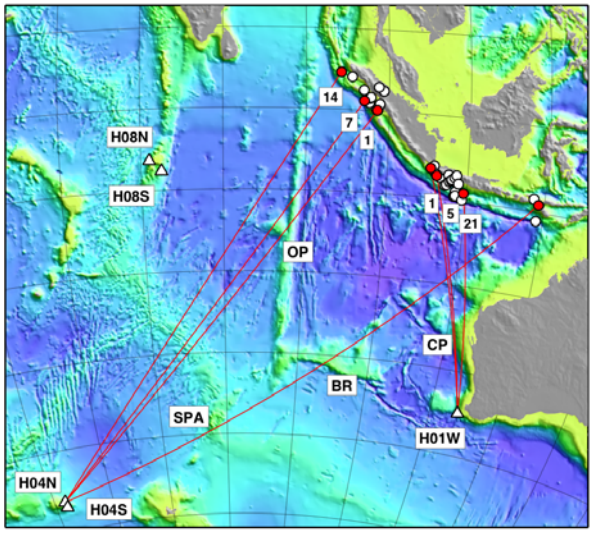

Figure 1. Earthquake and station locations. Hydrophone triads (triangles) and event locations (circles) are shown. Bathymetric features discussed in the text are also labeled: BR–Broken Ridge, CP–Cuvier Plateau, OP–Osborn Plateau, SPA–St. Paul-Amsterdam Plateau. Events plotted in red with ray paths are examined in more detail in the paper. The numbers along the ray paths correspond to event numbers used in the discussion.

Figure 2 shows the process used to estimate frequency-dependent signal loss. For each earthquake, the frequency spectrum of the direct T-phase recorded at H01W is compared with the spectrum recorded at H08S. The spectra are corrected for instrument response and a cylindrical spreading factor is included to account for the differing distances traveled from source to the different hydrophones. The signal loss estimation is considered valid where the signal level at H08S is 3 dB or greater above the noise level and the signal level at H01W is 1 dB or greater above the noise level. When the SNR at H01W falls below 1 dB, but there is still observable energy at H08S, then the estimated signal loss is considered a lower bound. The actual signal losses could be greater, but the noise level prevents us from knowing by how much. The same analysis is conducted for signals recorded at H04N.

Cuvier Plateau: Paths from the Java Trench to H01W

We selected events to provide a transect from west to east across the Cuvier Plateau that allows examination of T-phase attenuation as the water depth decreases. The event-station paths are shown in Figure 1. Figure 2 compares the signal received at H01W with the signal received at H08S for two events. The plots for event 1 show that frequencies below about 3 Hz are blocked by bathymetry along the path. For event 5, the corner of the attenuation plot moves to about 6 Hz, while all energy for event 21 (not shown) is blocked. We hypothesize that this blockage is due to the very shallow water depths (150 m) encountered along that path. By contrast, the shallowest water depth at the Cuvier Plateau for the path from event 1 is 2,600 m, and the shallowest depth for the path from event 5 at the Cuvier Plateau is 1800 m. This variation in the attenuation "corner frequency" implies that the Cuvier Plateau acts as a high pass filter with increasing higher frequency attenuation as the water depth decreases. Figure 3 shows the relationship between the mean attenuation between 1.5 and 4 Hz and the minimum water depth corresponding to the source-receiver path crossing the Cuvier Plateau. Figure 4 shows the plateau's bathymetry along a west-east transect with ray path crossing points color-coded by the attenuation corner frequency. We see from these figures that, in general, attenuation increases as water depth decreases. Once the water depth decreases to 1,000 m, nearly all T-phase energy is blocked.

These observations are complicated because attenuation determined for the paths might not be due solely to the Cuvier Plateau when the plateau's water depth is greater than about 1,200 m. The H01W bathymetry profiles in Figure 2 show that the ray paths cross shallow bathymetry (approximately 1,200 m) close to the hydrophones. Some signal is likely lost in this shallower water, and this may be the cause of some of the 1–3 Hz attenuation for events 1 to 6. This likely explains the nearly constant (and generally positive) level of attenuation for water depths at the Cuvier Plateau between 1,500 and 2,500 m in Figure 3.

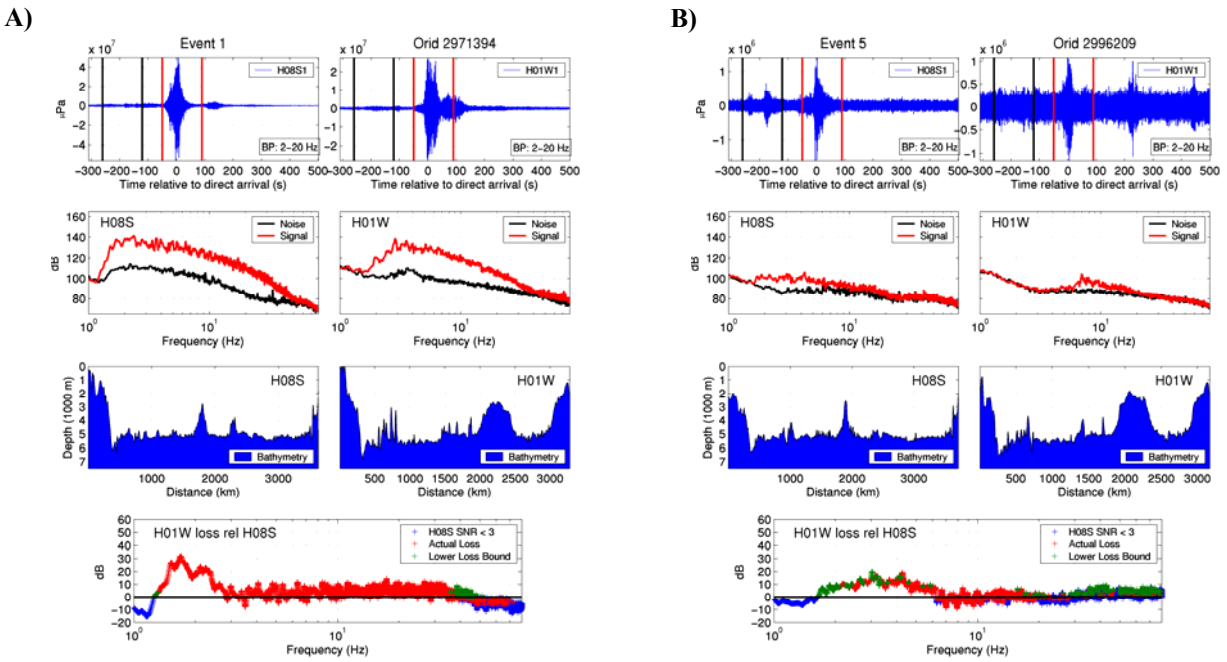

Figure 2. Signal loss for selected paths to H01W that cross the Cuvier plateau. Each sub-panel shows the waveforms at H08S1 and H01W1 (top panels), the triad-averaged signal and noise spectra (second row of plots), the bathymetry between the receivers and sources with the receivers on the right (third row of plots), and the computed signal loss at H01W relative to H08S (lowermost plots). Signal loss is color-coded. The three categories differentiate between valid signal loss estimations (red), lower bound signal loss estimations (green), and indeterminate estimates due to low SNR at H08S (blue). (A) The path for an event that crosses the Cuvier Plateau (distance from H01W is about 1,000 km) where the water depth is nearly 2,600 m, and frequencies below 3 Hz are blocked. (B) The path for an event that crosses the plateau where its depth is about 1800 m, and frequencies below 5–6 Hz are blocked.

We used RAM to estimate transmission loss between the Java Trench events and Cape Leeuwin. RAM is a parabolic equation code for computing range-dependent propagation loss (Collins, 1994). The along path environmental parameters were extracted from the World Ocean Atlas and the Sandwell and Smith global bathymetry database using BBN's Matlab interface HydroCAM. This implementation assumes a point source, which is not entirely appropriate for Java Trench earthquakes. To compensate for this approximation, transmission loss models were computed at several depths including the sound channel axis depth. Figure 5 shows results for a path that crosses the Cuvier Plateau for sources at 1,000 m and 2,000 m depths. For the 1,000 m depth simulation, which is near the sound channel axis, multiple modes are excited, but only mode 1 continues past the plateau. The deeper source excites a different set of modes, with what appears to be mode 2 continuing past the plateau. These indicate that all but the low-order modes will be stripped by the plateau bathymetry. For paths crossing over shallower portions of the plateau, the signal attenuation becomes highly dependent on bottom parameters. This is especially true for depths shallower than the sound channel axis because all modes will interact strongly with the seafloor. This leads to higher attenuation of the in-water signal due to energy leaking into the seafloor.

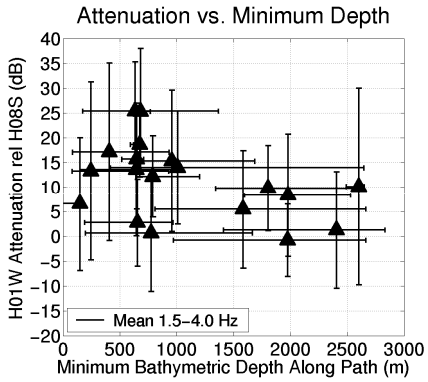

Figure 3. Attenuation vs. minimum depth at the Cuvier Plateau. The mean attenuation between 1.5 and 4 Hz is plotted. Vertical error bars represent two times the standard deviation, and horizontal error bars on bathymetry depth are computed by assessing the possible range of water depth that might be encountered given origin location errors.

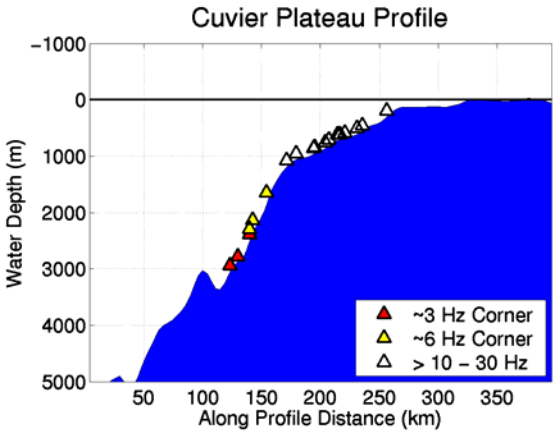

Figure 4. Changes in attenuation with bathymetry. The bathymetric profile for a transect across the Cuvier Plateau is shown (blue). The crossing points of rays to H01W are plotted as triangles color-coded to the corner frequency of the attenuation relative to H08S. The bathymetry of the Cuvier Plateau acts as a high-pass filter with increasing amounts of blockage as the water depth decreases.

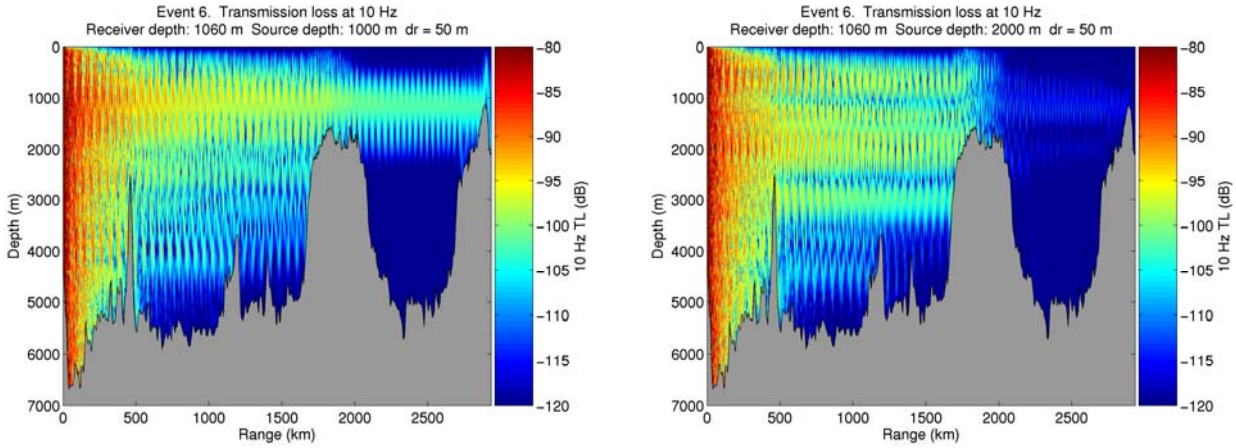

Figure 5. Transmission loss at 10 Hz modeled using RAM for a path from the Java Trench to H01W. Two different source depths are shown: 1,000 m (left panel) and 2,000 m (right panel). Propagation is dominated by mode 1 for the 1000 m source depth, while mode 2 and higher modes dominate for the 2000 m source depth. Interaction with the shallower bathymetry of the Cuvier Plateau at ranges 1,700–2,100 km increases transmission loss for both source depths, though the amount of transmission loss is greater for the deeper source.

Osborn Plateau: Paths from the Java Trench to H04N

Figure 6 shows attenuation observations for T-phases crossing the Osborn Plateau similar to the Cuvier Plateau results above. The mean attenuation in the 1.5 to 4 Hz band is shown versus the shallowest water depth encountered along path. There we focus on three events (see Figure 1). The path from event 1 crosses the eastern edge of the plateau, the path from event 7 crosses the middle of the plateau, and the path from event 14 passes to the north of the plateau. Attenuation is greatest for the path from event 7, and we hypothesize that the shallower water depth at the

Osborn Plateau is responsible for this attenuation. However, since the shallowest bathymetry encountered along this path is about 1,770 m, only energy between approximately 1 and 4 Hz is blocked. Higher frequency energy propagates over the plateau with little loss. Figure 6 shows a similar relationship as in Figure 3 with generally increased attenuation for shallower water. Also, the level of attenuation for 1,500 to 2,000 m water depths is similar, although the attenuation observations are complicated by near-receiver water depths of about 1,200 m.

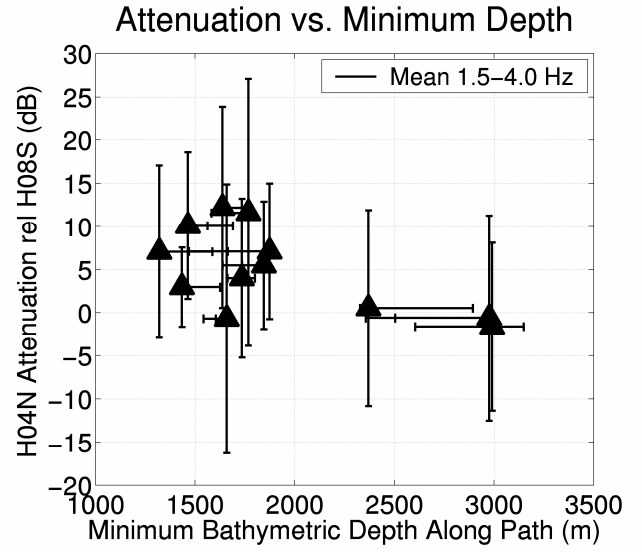

Figure 6. Attenuation vs. minimum depth for paths to H04N that cross the Osborn Plateau. Error bars are computed as in Figure 3.

Reflected Transmission Paths

A goal of this research is to correlate reflection strength to physical attributes of the reflector surfaces. Reflected signals were identified from several earthquake sources along the Java Trench at the Diego Garcia hydrophones. We used the direct arrival measurement seen at H08S and cylindrical spreading attenuation to normalize the other reflected signal strength and estimate reflection loss for different reflector surfaces. Reflector loss for various source reflector pairs were examined. However, the reflector strengths are highly correlated to the event location as opposed to the reflector location. Because the paths traverse deep water, we believe that this source dependence is more likely a function of the near-source hydroacoustic coupling than reflector attributes. The complicated nature of seismic-to-hydroacoustic coupling for trench events is well known (Graeber and Piserchia, 2004; de Groot and Orcutt, 2001), and it appears to dominate our observations, making trench events poor source candidates for this analysis. Instead we have analyzed several mid-ocean ridge events.

Signals from events along the Carlsberg Ridge northwest of Diego Garcia were studied for propagation and reflection loss characteristics. The events from this ridge are advantageous because their shallow locations and relatively simple bathymetry provide some of the most point like natural sources in the Indian Ocean basin (Hanson and Bowman, 2005). In addition many reflections from these events are commonly observed at the northern Diego Garcia triad. The shallow nature of the events and the proximity of the bathymetric ridge highs to the sound channel axis result in more high-frequency energy traveling through the SOFAR channel. Direct-T phases are often seen with energy at greater than 50 Hz. The reflection strengths also appear to be less source-dependent than for trench events.

Figure 7 shows events from the Carlsberg Ridge in the northwestern Indian Ocean that we examined for reflections. These events have clear paths to the northern Diego Garcia triad. Many reflections are observed from the surrounding continental slope and other prominent bathymetric features. Reflection losses were estimated for the 2 to 6 Hz frequency band by normalizing the reflected signal strength with the direct arrival and accounting for additional attenuation with distance. Reflector strengths are correlated by the reflector type/location although there is still scatter within each group (right panel). The differences in reflection strength within a group are most likely caused by differences due to near source bathymetry or earthquake source parameters, differences in the path attenuation of the direct source, and/or unresolved details in the reflector surfaces. The source coupling effect should be minimized because of the shallow nature of mid-ocean ridge earthquakes and the general coincidence of earthquakes with the shallowest bathymetry. The direct path attenuation might be significant because the source-to-receiver path often follows the relatively shallow and rough Carlsberg Ridge. However, if this factor was significant we would expect a decrease in inferred reflector loss for earthquakes occurring farther from H08N, which is not observed. Transmission loss along reflector paths should be minimal because reflector paths are generally orthogonal to the ridge and hence traverse fairly deep (nonattenuating) ocean paths. The possibility that the variation can be explained by more detailed reflector categorization is examined below.

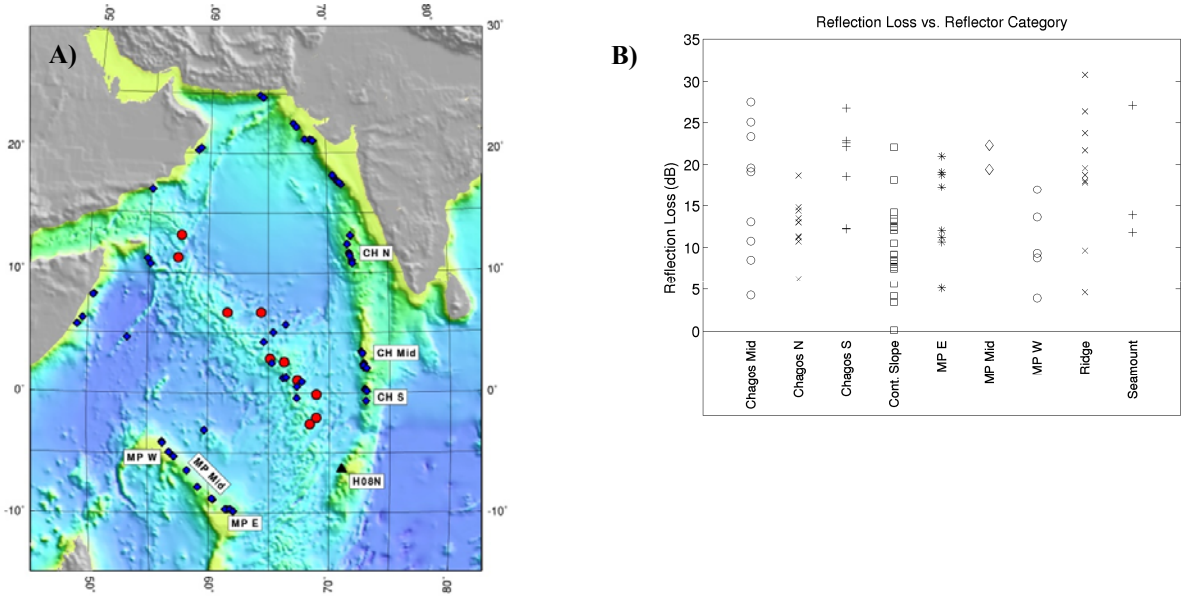

Figure 7. Reflection observations for events occurring along the Carlsberg Ridge recorded at H08N. A) Location map of earthquakes (circles) and reflection points (diamonds). The labels indicate groups of reflections. B) Reflection losses grouped by reflector category for the Carlsberg Ridge events. Reflector categories are defined by type (Continental Slope, Mid-Ocean Ridge, Seamount) or by geographic location (Chagos Archipelago north, middle, south and Mascarene Plateau (MP) east, middle, west). Losses are computed as the mean difference between reflected and direct arrivals in the 2–6 Hz band. Although each reflector category has a wide range of reflection losses, the continental slope reflectors show less signal loss than mid-ocean ridge reflectors. The Chagos Archipelago and Mascarene Plateau reflectors behave more like continental slope than mid-ocean ridge reflectors, probably due to their shallow bathymetry compared to ridges.

Reflections were analyzed for select Carlsberg ridge earthquakes described above. The time-bearing analysis of Hanson and Bowman (2006) was used to determine reflector locations based on azimuth and travel time estimates. The analysis estimated azimuths using a running 8 second time window with 50% overlap. Coherent arrivals that are continuous in the time-bearing domain were grouped together as a single reflector. An example from an earthquake that occurred in June 2003 is presented here. The reflectors found for this event are shown in Figure 8. This reflection analysis is only dependent on the earthquake location and time, the ocean sound speed, and the time-bearing measurements at H08N. At this stage information of the bathymetry has not been used. However, all reflector groups fall along distinct bathymetric features. By comparing reflections from a single source, we eliminate most of the source-dependent effects, especially the direct path attenuation. We compare these to reflection strength predictions estimated below.

Reflection strengths at H08N are predicted for a given source using the source/receiver geometry and bathymetric features. The reflections are clearly associated to bathymetric features. The analysis here attempts to establish how much of the reflector strength can be estimated from geometric factors computed from a global bathymetric map. We used the 2 minute resolution global bathymetric map of Smith and Sandwell (1997). Our analysis computed a reflector strength at each bathymetry point based on a composite of functions that depend only on the bathymetry, source location, and receiver location. These functions are blockage from source to reflector, blockage from receiver to reflector, depth relative to sound channel axis, reflector slope, transmission loss along source-reflector-receiver path, and a specular reflection coefficient. The strengths predicted from each function are multiplied to obtain a composite reflector strength.

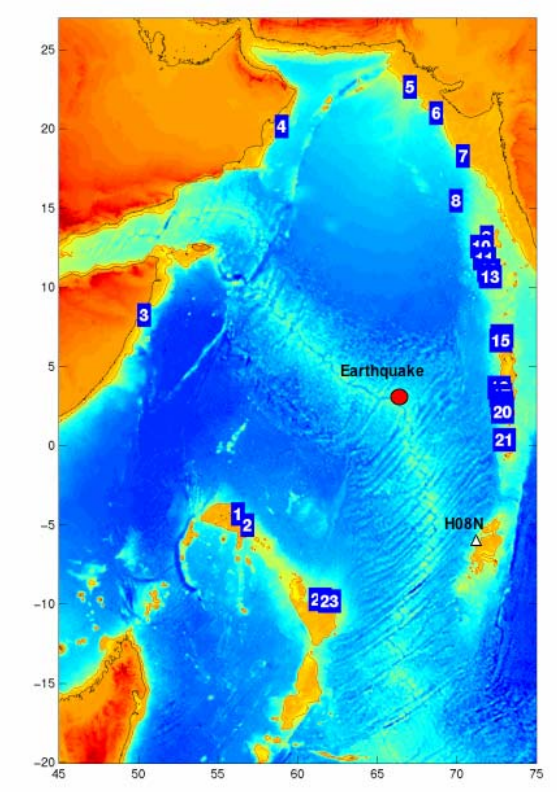

Figure 8. Map showing the inferred reflectors (numbers) of signals from a shallow earthquake on the Carlsbad Ridge (red circle) that occurred on June 22, 2003. Reflectors were identified based on the signal back azimuth measured at H08N and their time delay relative to the direct arrival.

These steps are demonstrated in Figure 9. Blockage is computed based on a bathymetric contour (currently 500 m). Two masks are computed with the source at center and the receiver at center. Instead of using a step function at the blockage contour, a 100 km transition zone is created using a sigmoid function. Reflection strength is assumed to be maximum at the sound speed channel axis. We assume the axis is a constant at 1200 m depth. The reflector strength is then estimated using a Gaussian centered on the axis. The width of the Gaussian is currently selected to be consistent with our general observations. The next factor affecting our prediction is the slope of the reflector. The slope is estimated at a particular bathymetry node in the database using the four closest nodes to compute an average slope. The cosine of the angle the normal makes with the horizontal is used to determine the slope's contribution to reflector strength with the constraint that the upward facing normal must be within 90 degrees of the reflector-to-receiver direction, i.e., the reflector must face the receiver. Finally, a reflection coefficient is computed that is a function of both the incidence angle from the source and the take off angle to the receiver. In purely specular reflection this function is zero when the incidence angle does not equal the take off angle. In purely diffuse reflection this function is independent of the take off angle. We compute a reflection function that allows for a trade-off between purely diffuse and purely specular reflection.

Figure 9 shows an example of estimating reflector strength from the various factors described above for the earthquake in Figure 8. The maps cover reflectors 9 through 13 in Figure 8. The depth based reflector strength function (Figure 9a) is necessary, but not sufficient in estimating the reflector strength. The inclusion of the bathymetric gradient and high specular reflectivity index explains many of the observed reflections. At this stage many of the strong reflectors that are predicted but not observed in the data are due to blockage.

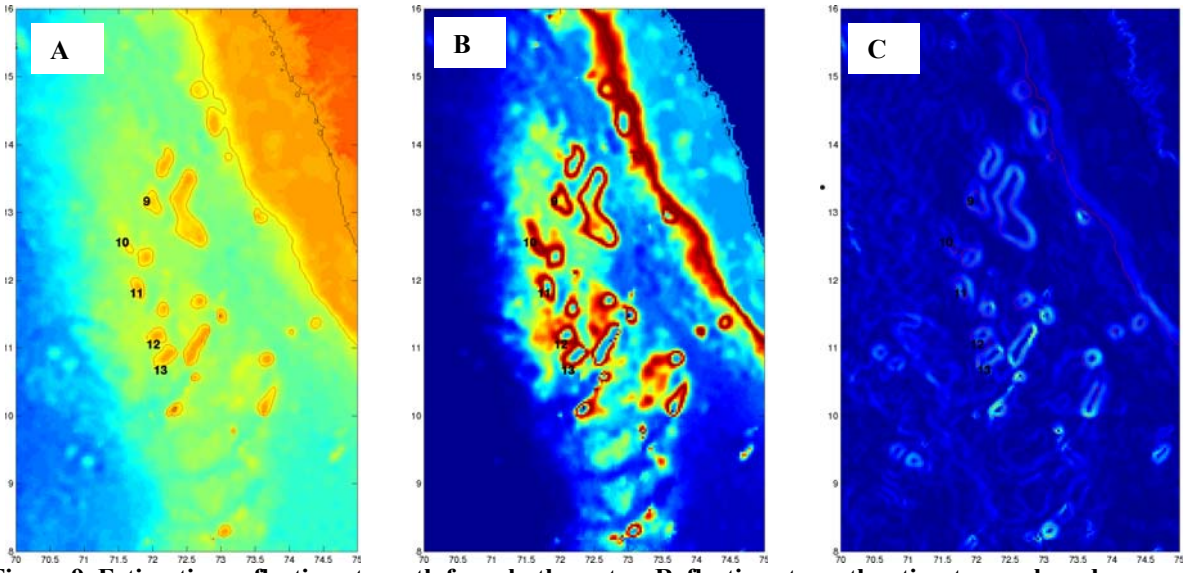

Figure 9. Estimating reflection strength from bathymetry. Reflection strength estimates are based on geometrical properties using the Smith and Sandwell (1997) global bathymetry database. The panels show some of the intermediate values that are used in estimating reflector strength. The bathymetry shown covers reflectors 9 through 13 from Figure 8. (A) Bathymetry with the 0 meter (black) and 1000 meter (red) bathymetry contours drawn. (B) Strength function based on water depth relative to sound channel axis. (C) Relative strength based on the average slope of the bathymetry.

The reflector strengths estimated at each bathymetry grid point are translated into an azimuth/time space corresponding to the expected angle and time of arrival at the hydrophone station. This results in a plot showing predicted arrival strength as a function of time and azimuth (Figure 10). This is compared to the measured angle of arrival with time from our standard time/bearing analysis (x's in Figure 10). Generally, measured arrivals coincide with the predicted energy. Energy arriving between 0 and 40 degrees corresponds to reflections from the Chagos Archipelago and the Indian continental slope. Energy arriving at 1,000 s between –120 and –60 degrees corresponds to reflectors from the Mascarene Plateau. However, there is also predicted energy with no corresponding observed arrivals. There are a number of reasons why this might happen. Energy arriving from different azimuth simultaneously will interfere with the coherence measures used to estimate azimuth. But the energy should be visible in an incoherent beam. This is not the case for the predicted energy arriving between 2,250 and 2,500 s, which corresponds to predicted energy from the coast of Africa. Because of the generally deep bathymetry, it is unlikely that this is due to unmodeled propagation loss. It is more likely that the continental slope in this area is a poor reflector.

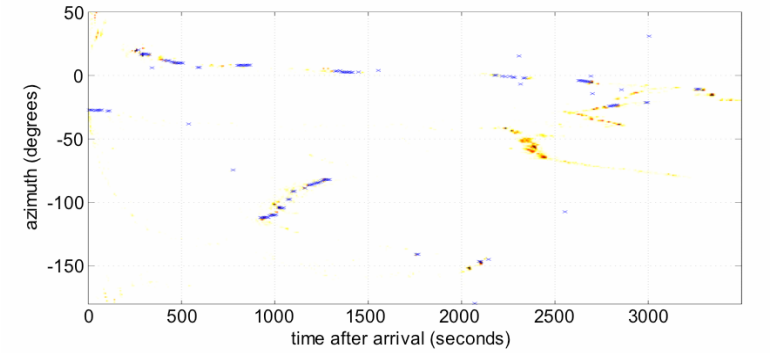

Figure 10. Comparison of predicted reflected energy (shading) and observed reflections (crosses) for the event in Figure 8. The shading represents predicted intensity based on bathymetry (dark red is high intensity, white is no energy).

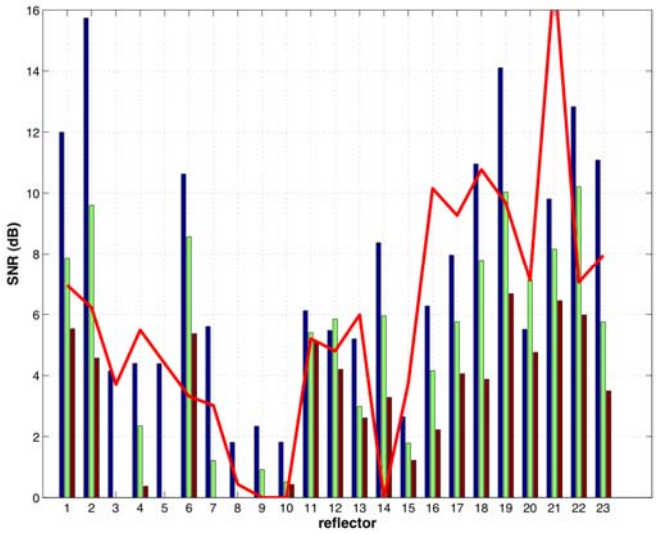

Figure 11. Histogram showing the signal-to-noise ratio (SNR) of reflected signals for 3–6 Hz (dark blue), 6–12 Hz (green), and 12–24 Hz (brown) frequency bands for the earthquake and numbered reflections in Figure 8. The red line shows the SNR predicted based on bathymetric factors. Low-frequency received levels are fairly consistent with prediction, with a few exceptions.

Figure 11 compares predicted reflection strengths versus observations with power spectra estimates. The bars represent observation power in three frequency bands. The red line is a relative measure of predicted reflector strength. Our predictions are frequency independent so there is only a single value per reflector. The predicted strengths correspond fairly well to the observations, especially considering the predictions have not included any sediment or surface roughness parameters.

The observations for each frequency band are represented as different color bars in Figure 11. The frequency bands are: 3–6 Hz, 6–12 Hz, and 12–24 Hz. The signal levels generally decrease with frequency as expected from the drop off in source level, but some reflectors lose more energy at high-frequency faster than others. This is independent of overall reflection strength levels. Figure 12 shows power spectra for the direct arrival and two reflections (6 and 7). The reflections are from two locations along the Indian sub-continent's continental slope. The frequency contents of the two reflections are strikingly different. The reflectors' surfaces are within 200 km of each other along steep portions of the continental slope. The major geometrical difference is the incidence and reflection angle between source and receiver. This difference may indicate a frequency-dependent scattering mechanism.

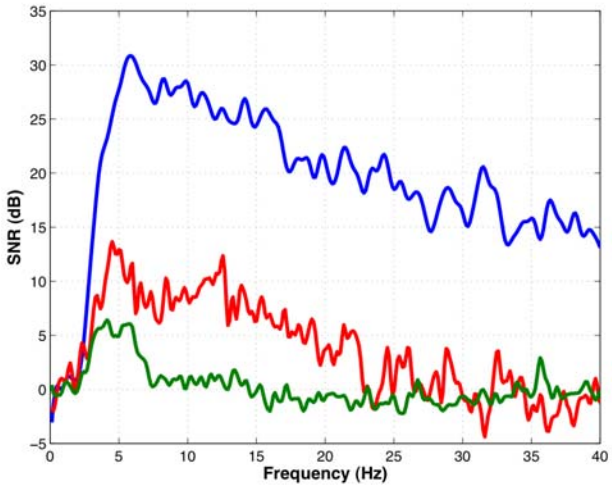

Figure 12. Power spectra for main and reflected signals. The blue line is an estimate of the power spectrum of the direct hydroacoustic arrival. The red and green lines are power spectra estimates for reflections 6 and 7 (from Figure 8), respectively. Note the difference in frequency content of the two reflections.

CONCLUSION AND RECOMMENDATION

We examined transmission and reflection losses for various source/receiver paths to better prepare for the Indian Ocean active source experiment. Natural sources were used in place of the controlled experiment sources. This limits the certainty that can be derived from the analysis. However, general conclusions can be reached. The experimental paths considered here appear to act as high pass filters with the corner frequency determined by the shallowest bathymetry along path. Higher frequency energy propagates over the bathymetric features relatively unattenuated until depths approach the SOFAR channel axis.

Many reflected signals have been observed. The trench earthquakes are not well suited for studying the properties of individual reflectors because the complicated hydroacoustic source region dominates the data variance. Ridge earthquakes are much better candidates for reflector analysis. Many reflections have been observed from Carlsberg Ridge earthquakes. The amplitudes of these reflected signals can be predicted to a large extent using simple functions that depend only on bathymetry, sound channel axis depth, and source and receiver locations. However, these predictions are not able to predict observed frequency variations, which may require the use of seafloor bottom properties.

ACKNOWLEDGEMENTS

We thank Dr. Jay Pulli and Mr. Zach Upton for their help in obtaining and running HydroCAM.

REFERENCES

Collins, M. D. (2004). Generalization of the split-step Padé solution, *J. Acoust. Soc. Amer.* 96: 382-385.

de Groot-Hedlin, C. D. and J. A. Orcutt (2001). Excitation of T-phases by seafloor scattering, *J. Acoust. Soc. Amer.* 109: 1,944–1,954.

Graeber F. M. and P.-F. Piserchia (2004). Zones of T-wave excitation in the NE Indian Ocean mapped using variations in backazimuth over time obtained from multi-channel correlation of IMS hydrophone triplet data. *Geophys. J. Int.* 158: 239–256.

Hanson, J. A. and J. R. Bowman (2005). Indian Ocean Ridge seismicity observed with a permanent hydroacoustic network, *Geophys. Res. Lett*. L06301, doi:10.1029/2004GL021931.

Hanson, J. A. and J. R. Bowman (2006). Methods for monitoring hydroacoustic events using direct and reflected T-waves in the Indian Ocean, *J. Geophys. Res*. doi:10.1029/2004JB003609.

Smith, W. H. F. and D. T. Sandwell (1997). Global seafloor topography from satellite altimetry and ship depth soundings, *Science* 277: 1957–1962.